The Flare Echo: Reflectivity and Velocity Signature

JAMES W. WILSON AND DARELYN REUM

National Center for Atmospheric Research, Boulder, Colorado*

(Manuscript received 12 March 1987, in final form 11 August 1987)

ABSTRACT

The characteristics and causes of a radar artifact called a flare echo are described. The spike or flare-shaped echo typically has reflectivities <20 dBZ_e and approaching Doppler velocities. It extends radially 10–20 km downrange of some intense radar storm echoes. Zrnić recently proposed a three-body scattering scenario to explain its occurrence, which consists of scattering by the hydrometeors to the ground, backscattering by the ground to the hydrometeors and scattering by the hydrometeors to the radar. In addition he developed relationships that predict the behavior of the flare reflectivities and velocities.

The data presented here support Zrnić's three-body scattering explanation and relationship, indicating that the flare echo power is dependent on the inverse cube of the distance from the large hydrometeors to the ground. The flare Doppler velocities depend on the radial velocity and fall speed of the hydrometeors responsible for producing the flare. However, it was found that Zrnić's theory did not fully address anomalies observed for scattering paths directly below the large hydrometeors and the contribution of their radial velocities to the flare velocities.

In this paper flare echo data from Colorado and Alabama are compared. The Colorado flares are typically more intense, extensive, and longer lasting and are highly likely to be associated with large (≥2 cm) hail and can thus be used as a warning signature. However, this use is not transferrable to Alabama storms where surface hail rarely occurs with flare echoes. In fact, there is evidence that large raindrops may sometimes cause the flare in Alabama.

The flare echo may cause difficulties for unaware researchers using multiple Doppler techniques to synthesize wind fields. It is also a potential problem for forecasters interpreting the data and computer algorithms searching for velocity features such as downbursts and gust fronts. The flare velocities may prove useful for nowcasting microbursts.

1. Introduction

An elongated radar reflectivity and Doppler velocity signature resembling a spike or flare (see Fig. 1) has been observed to extend radially outward beyond some strong radar echoes. The signature which we chose to call a "flare echo," typically extends 10–20 km from the back edge of the cell and exhibits reflectivities ≤20 dBZ_e.[1] The Doppler velocities within the flare are usually toward the radar and have been observed to be as strong as 20–40 m s^{-1}. Figure 1, a black and white photograph showing reflectivities associated with a flare that occurred on 13 June 1984 near Denver, Colorado, was taken when the flare was at maximum length; at this time, golfball-size hail was reported at the surface. This signature is not likely the same as the hailfinger signature reported by Battan (1973). The hailfinger, while not well defined, may include real precipitation or sidelobe echo and may have any orientation, while the signature presented in this paper is an artifact and has a specific orientation.

The flare echo was first noted by the first author on 24 June 1982 during the Joint Airport Weather Studies (JAWS) project from the National Center for Atmospheric Research (NCAR) 5- and 10-cm wavelength Doppler radars. A research aircraft in the vicinity reported a hail swath on the ground from the storm producing the flare echo and public reports indicated 1 in. (2.5 cm) diameter hail on the ground, 5 in. deep. In the 1984 Convection Initiation project in Colorado and in the 1985 PRESTORM project in Kansas, flare echoes were again reported with large and damaging hail. Wilson and Reum (1986) originally called this signature a "hail spike" based on studies from Colorado which showed a close relationship with large surface hail. However, after it was observed in the absence of surface hail during the Microburst and Severe Thunderstorm (MIST) Project in Alabama, Professor Theodore Fujita suggested it be renamed a flare. This paper extends the studies of Wilson and Reum (1986) to include data from Alabama with the purpose of docu-

* The National Center for Atmospheric Research is sponsored by the National Science Foundation.

[1] Z_e refers to the effective radar reflectivity factor. This means the reflectivity is equivalent to that from raindrops scattering in the Rayleigh region where the complex refractive index is equal to 0.93.

Corresponding author address: Mr. James Wilson, NCAR/AID, P.O. Box 3000, Boulder, CO 80307.

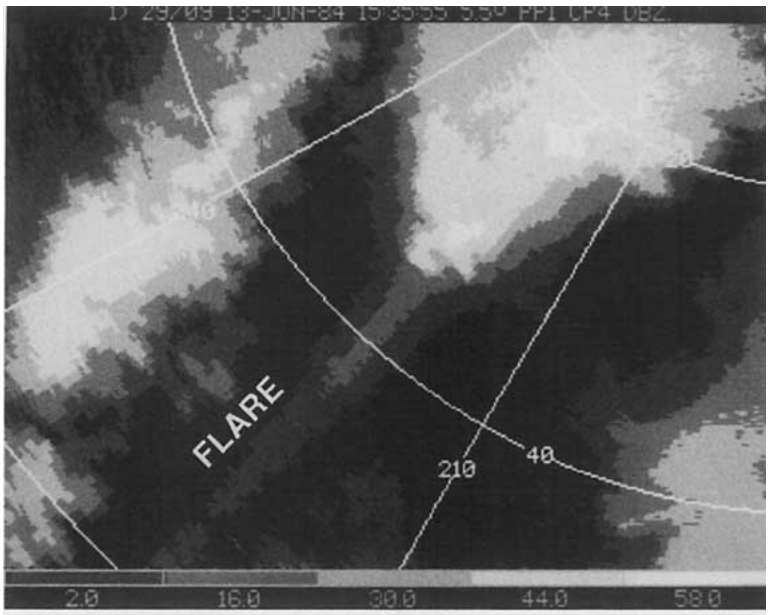

FIG. 1. The PPI radar reflectivity display of a flare echo as observed by CP-4. The reflectivity in dBZ_e is given in seven shades of gray by the scale at the bottom. This storm produced extensive hail damage in Denver, Colorado at 1535 MDT 13 June 1984. Range marks are at 20 km intervals and the antenna elevation angle is 5.5°.

menting the characteristics of this radar signature, establishing its origin, and determining its meteorological significance.

Zrnić (1987) proposes a three-way scattering mechanism to explain the phenomena. This theory is presented in section 2. Section 4 compares flare characteristics from Colorado and Alabama, and section 5 provides comparisons of hail events and flares, including dual-polarization data for differentiating precipitation type. Section 6 compares theory and observations.

2. Theory

Zrnić (1987) observed flare echoes with the National Severe Storms Laboratory 10-cm wavelength radars in Oklahoma. He attributed the echoes to a three-body scattering process that involved, first, scattering of electromagnetic fields by large hydrometeors to the ground; second, backscattering by the ground to the hydrometeors; and third, scattering back to the radar antenna. This three-body scattering process is illustrated in Fig. 2. This illustration is based on a range–height indicator scan (RHI) taken during the MIST project for a thunderstorm that produced a flare. The radar signal strikes large hydrometeors at point C, a distance R from the radar. Large hydrometeors, portrayed by the shaded region near point C in Fig. 2, cause strong scattering toward the ground. The scattered signal from the large hydrometeors strikes the ground in a broad circular region under the storm. The signal is then reflected from the ground, some of which once again strikes the large hydrometeor region, with some of the energy returning to the radar. Figure 2 shows the path of this signal. Depending on the scattering paths angle of incidence with respect to the ground (θ_r), the signal will travel a distance r from point C to the ground. All possible paths from point C with the same θ_r strike the ground along the dashed circle in Fig. 2. Signals following these paths will travel a total distance of $2(R + r)$ and will arrive at the radar simultaneously and be displayed a radial distance $R + r$ from the radar. The shortest path, or the fastest

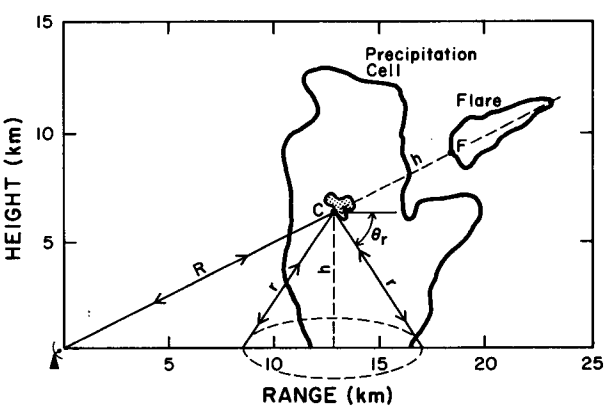

FIG. 2. Schematic of the proposed radar signal path responsible for the flare echo. The precipitation cell and flare are as observed by CP-4 on 20 July 1986 near Huntsville, Alabama. The dark shading near point C represents the 60 dBZ_e core responsible for producing the flare echo. See text for further description.

time of arrival, will be for vertical paths directly below the strong scatterers ($\theta_r = 90°$). This path is marked with an h in Fig. 2. For the radial beam shown in Fig. 2, the flare would begin at point F, a distance h from point C. Other paths for $\theta_r < 90°$ will be displayed along the radial at increasing distance beyond F as θ_r decreases. Since Fig. 2 is based on actual data, the fact that the flare begins at a radial distance beyond the core that is equal to the height of the core above ground is strong evidence that the flare is caused by backscattering from the ground.

Zrnić developed a radar equation for this three-body scattering process that states that the echo power in the flare region is dependent on r^{-3}, i.e., the received power decreases with the inverse cube of the distance from the strong scatterers to the ground (see Appendix). Based on observed reflectivity values in the flare region, Zrnić concluded that the flare was caused by non-Rayleigh scattering from large hydrometeors which were most likely water-coated hail.

In developing the equation for the reflectivity in the flare region, Zrnić assumed the backscattering cross section of the ground to have only a weak dependence on θ_r. Long (1975) shows that for many ground features and radar wavelengths the cross section increases significantly for θ_r near 90°. Section 6 expands upon cases where the r^{-3} dependence for the flare echo does not hold when θ_r is near 90°. Actually, Zrnić has treated the case for $r > h + d$ (d is the depth along the beam axis of the region of hydrometeors that produce the flare) where the contribution from the near vertical incident paths is not contributing to the flare reflectivity.

Zrnić proposed that the Doppler velocity within the flare (V_f) depends on the vertical motion (W) and the radial velocity (V_r) of the scatters. Assuming the energy is scattered equally in all directions, i.e., the power received from the ground at C is equal for all paths of constant r, then

$$V_f \approx V_r + W \sin\theta_r. \quad (1)$$

The flare velocity actually depends on an additional term not shown in Eq. 1 (Zrnić, personal communications). This term is $V_r \cos\theta_e \cos\theta_r$, where θ_e refers to the radar antenna elevation angle. This term was not originally considered by Zrnić, since its total contribution would be zero for each scattering volume if the signal return from each path about the ground circle in Fig. 2 were equal. This is because the sign of the term will reverse from one side of the circle to the other. However, this term will have the effect of producing a broad, flat Doppler spectrum, particularly when V_r is either a large negative or a positive value and when $W \sin\theta_r$ is small. For this situation, which would be common at the farther end of the flare, the computed mean Doppler velocity by a pulse-pair processor is likely to be quite noisy and will tend toward zero even though V_r is nonzero.

3. Data

The NCAR CP-2 and CP-4 radars were used for this study. The CP-2 is a dual wavelength (10.7 and 3.2 cm) and dual polarization Doppler radar. The CP-4 radiates at a 5.4 cm wavelength. In all cases the polarization was horizontal. Radar characteristics are given in Table 1.

Data for this study are from three convective storm seasons: 1983, 1984, and 1986. The 1983 data were from the 10-cm wavelength system of the CP-2 radar which was located 25 km east of Boulder, Colorado during the Program for Regional Observing and Forecasting Services (PROFS) experiment. The 1984 data were from CP-4, which was located 5 km west of Brighton, Colorado, during the May Polarization Experiment (MAYPOLE) and the Convection Initiation Project. The 1986 data were from both CP-2 and CP-4 radars located, respectively, 25 km northwest and west of Huntsville, Alabama during the MIST project.

Flare echoes from 24 Colorado and seven Alabama cases were examined. A systematic search for Colorado flare echoes was based on first recording the time and location of surface reports of hail $\geq$ 2 cm and then searching the radar data tapes for corresponding echoes. This approach was instituted because of the original desire to determine if the flare echo was associated with large hail. Selection of flare echoes from Alabama was based on field records noting their presence. Many other flare echoes exist in the Alabama dataset; however, the characteristics of the flares presented in section 4 are representative of Alabama flares in general.

4. Flare echo characteristics

Table 2 shows flare echo characteristics from Colorado and Alabama as observed by CP-4 radar. The radar range of the storms are between 18 and 65 km. The Colorado data, Table 2a, are from 3 days where the complete evolution of eight flares could be studied. Similar statistics for seven cases from 4 days in Alabama are given in Table 2b.

Values for the core reflectivity, flare reflectivity, flare length, flare velocity, and flare vertical extent represent the maximum measured during the lifetime of the flare. The flare heights given in the last three columns in Table 2 indicate the height of the storm reflectivity core which is causing the flare, not the height where the flare is observed. The maximum flare velocity refers to the maximum approaching velocity. Receding velocities within the flare are rare. As will be discussed in section 6, approaching velocities are much more frequent than receding because of the greater magnitude of particle fall speeds over the air motions.

a. Colorado

For Colorado, the maximum length of the reflectivity flare and the maximum approaching Doppler velocity

TABLE 1. Radar characteristics for given radar and year.

	CP-2 (1986)	CP-2 (1986)	CP-4 (1986)	CP-4 (1984)	CP-2 (1983)
Wavelength (cm)	10.67	3.2	5.49	5.49	10.67
Half power beamwidth (deg)	0.93	0.94	1.1	1.1	0.96
Average transmitted power (dB m)	59	43	55	55	60
Pulse width (μsec)	1.0	1.0	1.0	1.0	1.0
Radar system[1] gain (dB)	42.6	44.0	42.1	42.0	42.2
Log receiver threshold power (dB m)	−110	−113	−112	−106	−110

[1] Includes waveguide loss.

varied from 4–30 km and 10–43 m s^{-1}, respectively. The lifetime of the flare varied from 11–68 min. The height of the reflectivity core varied from the surface to 9.5 km. Also, the height of first appearance varied considerably from near surface to 7.4 km. While the precipitation core causing the flare was frequently observed to first begin above the freezing level and descend with time, there was no consistent pattern. For the cases presented in Table 2a, the height of the freezing level was between 2.4 and 2.7 km above ground.

In the eight cases, 63 volume scans contained flares. Maximum reflectivities per volume scan varied from 45–65 dBZ_e and flare lengths from 1–30 km. However, there was no correlation between the two variables. The exact meaningfulness of the observed core reflectivities is questionable because there was often considerable attenuation in these storms, and the scatterers are presumably non-Rayleigh targets.

b. *Alabama*

Field experience indicated flare echoes were more common in Alabama than in Colorado but were very seldom associated with surface hail in Alabama. Table 2b shows the Alabama flares, on average, have smaller lengths, smaller reflectivities, smaller approaching velocities and shorter lifetimes than Colorado flares. None of the Alabama flare-causing cores were observed below

TABLE 2. Flare echo characteristics for Colorado and Alabama.

Date	Max core reflectivity (dBZ_e)	Flare max reflectivity (dBZ_e)	Flare max length (km)	Flare max velocity (m s^{-1})	Flare lifetime (min)	Flare† lowest height when first observed (km)	Flare† lowest height observed (km)	Flare† highest height observed (km)
				(a) Colorado				
12 June 1984A	50	10	11	25	18	<0.4	<0.4	3.6
12 June 1984B	55	10	5	30	31	3.0	<0.3	6.2
12 June 1984C	60	29	30	43	48	7.4	<0.2	7.4*
13 June 1984A	60	23	18	30	44	3.2	<0.4	9.5*
13 June 1984B	60	25	20	35	68	4.2	<0.2	7.3*
13 June 1984C	65	30	12	38	60	1.7	0.8	5.5
15 June 1984A	60	15	10	10	11	2.0	1.4	3.6
15 June 1984B	60	5	4	23	17	3.9	1.1	3.9
Average	59	18	14	29	37	3.2	<0.6	5.9
				(b) Alabama				
3 June 1986A	65	15	13	26	10	3.3	1.1	6.5
3 June 1986B	65	10	13	26	44	3.2	1.7	7.0
3 June 1986C	60	5	10	22	15	4.2	3.2	6.5
3 June 1986D	60	15	10	22	15	3.8	1.0	6.5
1 July 1986	60	10	12	24	12	4.7	2.1	6.9
13 July 1986	65	15	13	26	20	4.5	1.1	8.2
19 July 1986	65	10	7	16	19	1.7	1.2	6.1
Average	63	11	11	23	19	3.6	1.6	6.8

* Maximum height scanned by radar.
† Refers to the height of storm reflectivity core that is causing the flare.

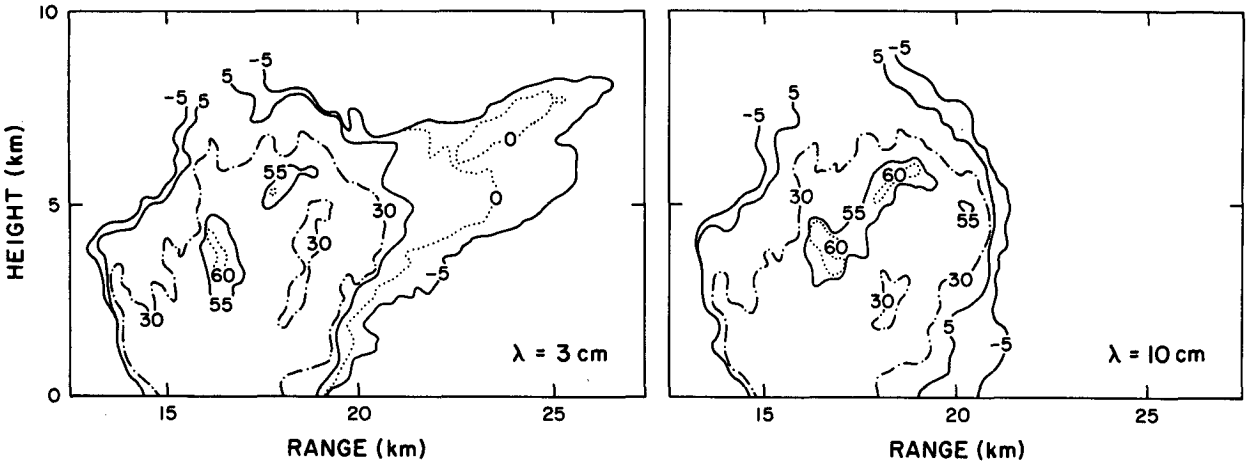

FIG. 3. Comparison of RHI displays from CP-2 of radar reflectivity for the 3- and 10-cm wavelengths. Data are from 1 July 1986 at 1611 EDT near Huntsville, Alabama for the 310° azimuth.

1 km even though the radar was able to observe nearly to the surface, while in Colorado it was common for this core to reach the surface. When the core causing the flare was first observed, it tended to be above the freezing level in Colorado and to straddle the freezing level in Alabama. The freezing level was typically 5 km and 2.5 km above ground for the Alabama and Colorado cases, respectively.

c. *Wavelength dependence*

The statistics in Table 2 are based on 5 cm wavelength data. From field experience, it is obvious that the flare echo was more prominent and occurred more frequently at shorter wavelengths. This is particularly obvious when CP-2 3-cm and 10-cm data are directly compared. Figure 3 shows a well-developed flare on the 3-cm wavelength display that is absent on the 10-cm wavelength. In fact, while numerous flare echoes were observed at 5 cm and 3 cm in Alabama, they were rare and generally quite weak at 10 cm. The greater propensity of flares at shorter wavelengths suggests the flare may be caused by non-Rayleigh scattering.

5. Associated precipitation

a. *Surface hail reports*

The 1983 and 1984 Colorado data were examined to determine the correspondence between surface hail and the occurrence of a flare echo. The 1984 hail reports were from Storm Data[2] for the period 18 May–13 August. The analysis consisted of plotting all reports of hail ≥ 2 cm within 70 km of the radar on a base map. The radar data were then searched for corresponding echoes. With the exception of the immediate vicinity of Denver, the area is very sparsely populated and experience has shown a large number of hail occurrences go unreported. Also errors in time and uncertainty in reported locations make the Storm Data reports difficult to use. During the PROFS experiment in 1983, the Storm Data reports were supplemented by three chase cars that were directed to potentially severe storms using radar information for guidance.

A total of 71 large (≥2 cm) hail events were identified for which corresponding radar data existed. A continuous surface hail swath defined a single event. Fifty-eight events were identified in 1983 compared to 13 in 1984 because of a more continuous radar dataset and the addition of PROFS verification spotters. Table 3 is a summary of the occurrence of flare echoes with large hail events for each year.

Table 3 shows that 6 of the 13 hail storms in 1984 produced flare echoes. It is possible that flares occurred with the other seven cases but were masked by a stronger echo. In five of the null cases other storms were located immediately behind the hail producing echo. In the other two null cases a substantial second trip echo masked the area where the flare would be expected. While searching the radar data, two additional storms were observed to contain flare echoes. No surface reports of hail were associated with these storms.

TABLE 3. Number of flare echo observations associated with large (≥2 cm) hail.

	CP-2 (10 cm) 1983	CP-4 (5 cm) 1984
Large hail cases	58	13
Flare observed	18	6
No flare observed/obstruction	30	7
No flare	10	0

[2] Available from National Climatic Data Center, National Environmental Satellite, Data Information Service, NOAA, Federal Building, Asheville, NC 28801-2696.

However, they occurred in remote areas where receipt of reports was unlikely.

Table 3 indicates 18 of the 58 large hail events in 1983 had associated flare echoes and 30 could have been masked by stronger echo. In contrast to 1984, no flare was observed for 10 cases, even when no obscuring phenomena was present. Remember that the 1983 data was based on 10-cm wavelength radar data as compared to 5-cm data in 1984. As discussed in subsection 4c, flare echoes are more common at shorter wavelengths.

Because of inaccuracies and incompleteness of the surface hail reports, it was impossible to compare the evolution of the flare with precise hail events on the ground. Nor was it possible to definitively conclude what relationship exists between surface hail and the flare echo. However, there was strong evidence that in Colorado the two were highly correlated, particularly for 5-cm wavelength radars.

The Alabama flare echoes were not associated with significant hail at the surface. In one case (Fig. 7) a research vehicle observed pea-size hail mixed with heavy rain. The lack of surface hail doesn't necessarily mean that hail did not cause the flare, since it could have melted before reaching the ground. Table 2b shows the high-reflectivity cores associated with flare echoes were not observed below 1 km. The higher freezing level and higher-humidity environment in Alabama significantly reduces the chance of hail reaching the ground. The higher humidity reduces evaporation and results in higher relative temperatures in the hail core.

b. Dual-polarization indications

Dual-polarization data were available during MIST for the 10-cm system of CP-2. The ratio of the received power from horizontally and vertically polarized radar signals is referred to as differential reflectivity (Z_{DR}). A variety of studies have shown horizontal reflectivity (Z_H) and Z_{DR} are effective in discriminating hail from rain (Leitao and Watson 1984; Bringi et al., 1984; Aydin et al., 1986; and Lipschutz et al., 1986). In general, high-reflectivity factors coupled with Z_{DR} value near zero indicate hail, while positive Z_{DR} values indicate rain. Hail–rain discrimination curves from Aydin et al. (1986) indicate rain for Z_{DR} values > 1 dB at Z_H = 45 dBZ_e. This discrimination point increases to >2 dB at 60 dBZ_e. Above 60 dBZ_e data are lacking but extrapolation of the curve indicates the rain–hail discrimination curve would suggest rain for Z_{DR} values > 2.5 dB at 70 dBZ_e.

Utilizing the CP-2 Alabama dataset, Z_{DR} values for storm cores that produced flare echoes were examined. Flare echoes were associated with Z_{DR} values between 0 and 5 dB. Thus it is likely that the larger Z_{DR} values were associated with rain cores. The case shown in Fig. 3 is particularly suggestive of a rain core. Except for echo < 30 dBZ, this storm did not grow above 7 km. The freezing level was near 5 km. Throughout the evolution of this storm the Z_{DR} values within the high-reflectivity region of the storm were between 2 and 5 dB. This indirect evidence suggests the temperature in the updrafts remained above freezing and that rain was produced by the warm rain process.

A definitive conclusion on the precipitation type associated with the flare echo is not possible. However, the data seem to suggest that flare echoes can be caused by either hail or rain. The evidence indicates hail is the predominant cause in Colorado. However, in Alabama large raindrops are likely the cause, at least in some instances. This is suggested by the relatively low flare reflectivities, short flare lengths, high core reflectivities, rare flare occurrence at 10-cm wavelength radar and often positive Z_{DR} values.

6. Observation and theoretical comparisons

The data collected with the NCAR radars in Colorado and Alabama can be used to test some of the theoretical concepts presented by Zrnić. The following theoretical premises are examined in this section: (a) the flare results from three-body scattering; (b) the echo power in the flare depends on r^{-3}; and (c) the velocity in the flare is predicted by Eq. (1). Two other hypotheses presented by Zrnić have already been examined in earlier sections. These are that non-Rayleigh scattering causes the flare and the scatters are most likely wet hail.

Figure 4 is a plot of the reflectivity and velocity as a function of range for the 220° azimuth in Fig. 1 that

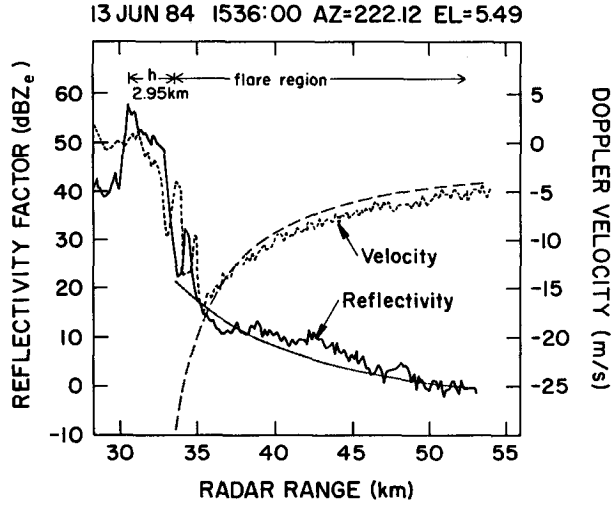

FIG. 4. Reflectivity and Doppler velocity as a function of radar range through the flare echo in Fig. 1. Data taken by CP-4 on 13 June 1984 at 1536 MDT near Denver, Colorado for an azimuth of 222.12° at an elevation angle of 5.49°. The heavy solid line and dashed heavy line are reflectivity and Doppler velocity, respectively. The light solid curve and light dashed curve are approximate theoretical fits to the data (see text). The vertical distance from the core center to the ground is indicated by the letter *h*. The predicted flare region is also indicated.

traverses the flare. The height of the 58 dBZ_e core above the ground is 2.95 km. Based on the three-body scattering discussion in section 2, the flare was first observed 2.95 km beyond this core. However, in this case, a precipitation echo is still present at this range and the flare first becomes visible at a range of about 35 km (~5 km beyond the core). A curve representing the predicted r^{-3} dependence of the flare echo power is overlaid with the observations. Actually, the curve represents $(R + r)^2 r^{-3}$, since reflectivity factor is plotted instead of received power (see Appendix). The procedure was to fix the down-range end of the curve to the observations. Then the suitability of r^{-3} would depend on the fit of the observations to the rest of the curve. In this case the fit is fair, underestimating observations slightly between 39 and 46 km.

The radial velocity within the core is near zero ($V_r = 0$); thus, Eq. (1) would predict the flare velocity would depend on $W \sin\theta_r$. Values of W were tested until a best fit to the observations was attained. For this case, $V_f = -30 \sin\theta_r$ resulted and is shown in Fig. 4. This curve tends to overestimate the observations, however; subtracting 1 from this equation, which would be equivalent to assigning $V_r = -1$ instead of 0, results in a close fit to the data. This indicates that the fall speed of the flare-causing scatters is ~30 m s^{-1}. Unless there are significant downdrafts, large wet hail would be required to obtain such a large fall speed (Ulbrich, 1977). This case tends to support the three-body scattering concept and the equations proposed by Zrnić for the flare reflectivity and velocity. However, this is not to say that other curves might not fit the reflectivity data better.

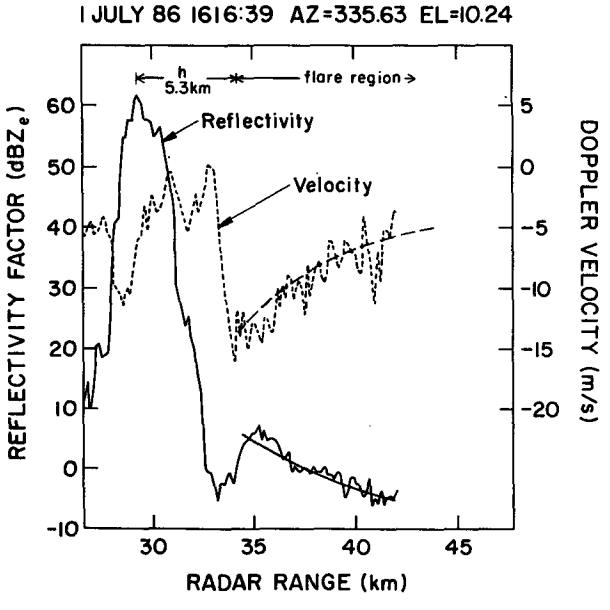

FIG. 5. As in Fig. 4 except for a flare echo on 1 July 1986 at 1616 CDT near Huntsville, Alabama, for an azimuth of 335.6° and elevation angle of 10.24°.

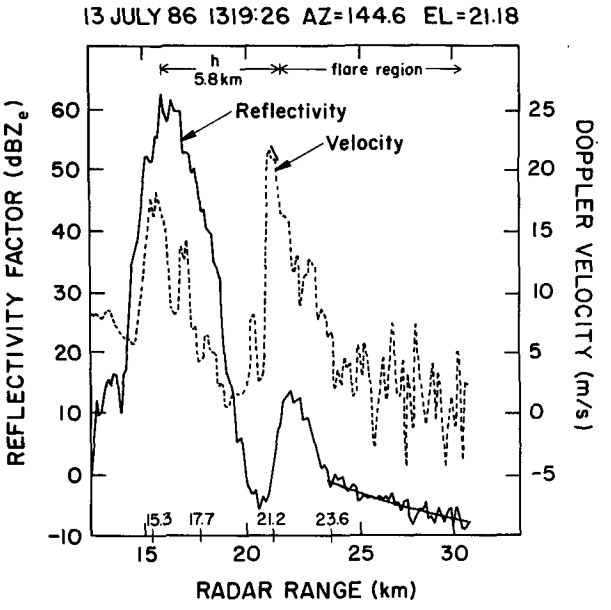

FIG. 6. As in Fig. 4 except for a flare echo on 13 July 1986 at 1319 CDT near Huntsville, Alabama, for an azimuth of 144.6° and elevation angle of 21.18°.

Two other examples similar to Fig. 4 of the reflectivity and Doppler velocity through a high-reflectivity core and corresponding flare are given in Figs. 5 and 6. These cases are from the MIST project in Alabama using the CP-4 radar. These two cases were selected because of substantial nonzero radial velocities within the core regions. In the 1 July case (Fig. 5) the radial velocity varies from −11 to 0 m s^{-1} across the 50 dBZ_e core, with a value of −6 m s^{-1} at the 61 dBZ_e center.

Figure 5 shows that for both velocity and reflectivity the flare starts ~5.3 km beyond the maximum core reflectivity. Again this distance is about the height of the core above the ground. The thick solid curve in Fig. 5 shows the flare reflectivities decrease approximately as r^{-3}. This time the fit is better than in Fig. 4. The best fit to the velocity observations is $V_f = -15 \sin\theta_r$ (thick dashed curve). It is surprising that this velocity curve fits the observations, since the V_r term is zero even though significant negative radial velocities exist in the core. In this case it would appear the core radial velocities do not contribute to the flare velocities.

The flare in Fig. 6 behaves considerably different than the others already presented. The flare reflectivities and velocities between ranges 21.2 and 23.6 km essentially mirror those of the storm core between 15.3 and 17.7 km. The height of the core in Fig. 6 is ~5.8 km which is the distance downrange that the core reflectivities are reproduced. This mirroring of the core in the flare region is even more apparent when viewing the full RHI from which Fig. 6 is extracted. As discussed in section 2, the vertical incident path ($\theta_r = 90°$) is dominating all other paths apparently because the radar

cross section increases significantly for θ_r near 90°. In this mirror region of the flare the reflectivities in this case are ~49 dB less than the core reflectivities. Beyond the mirror region, the flare reflectivities in this case follow the r^{-3} relationship as indicated by the solid curve.

The precipitation core velocities and associated mirrored flare velocities are quite similar except the flare velocities are ~4 m s^{-1} larger for the first peak; this indicates the particle fall velocities are upward at 4 m s^{-1}, indicating a significant updraft. Beyond the mirror region the flare velocities become noisy and approach zero.

Visual examination of the cases used in Table 2 indicates the $W \sin\theta_r$ term usually dominated the flare velocities. However, it was observed on occasions that the core radial velocities contributed significantly to the velocities in the flare as would be expected from Eq. (1). The flare velocities at the far ranges of the flare became erratic and approached zero rather than the core radial velocity as predicted in Eq. (1). This is likely a result of large velocity spectral widths at these ranges that resulted in the radar processor computing a mean Doppler velocity near zero. This possibility was discussed in section 2.

Positive flare velocities are seldom observed presumably because the fall speed of the scatterers are predominately downward (Fig. 6 is a notable exception). Figure 7 shows the evolution of a flare where the core and flare initially grow upward and then rapidly descend. The corresponding flare velocities, within a period of 7 min 40 sec, change from initially all positive (max + 16 m s^{-1}) to all negative (min −20 m s^{-1}). During the same period, the core velocities only changed from an average +4 m s^{-1} to −3 m s^{-1}. It appeared the flare velocities were dominated by the $W \sin\theta_r$ term, as W evolved from positive to negative in response to a strong updraft changing to a downdraft.

The above indicate that both the vertical component of the scatter velocities and their radial velocities contribute to the flare velocity. However, when the core velocities are significantly nonzero, apparent broadening of the Doppler spectrum and variations in the radar cross section of the ground cause unpredictable results.

7. Conclusions

A radar artifact in reflectivity and Doppler velocity, which we call a flare echo, appears to be caused by scattering from large hydrometeors. The signature appears as a low-reflectivity (typically <20 dBZ_e) spike or flare-shaped echo extending radially downrange beyond some intense storms. The Doppler velocities in the flare are usually approaching the radar with maximum values (typically >15 m s^{-1}) near the leading edge of the flare echo.

Zrnić (1987) proposed that this signature results from a three-body scattering phenomena caused by non-Rayleigh scattering from large hydrometeors—most likely large wet hailstones. The observation that the flare starts at a radial distance downrange from the core that is equal to the core's height above ground is strong support for this concept. The data also tend to support Zrnić's conclusion that the reflectivity in the flare decreases with the inverse cube of the slant distance from the hail core to the ground. However, there is sometimes a region of the flare corresponding to ground-scattering paths with near vertical incidence, where the core reflectivities are reproduced with a near constant reduction in value. We refer to this as the mirror region. Zrnić also developed a relationship for the velocities in the flare region that depends on both the radial velocity and fall speed of the flare producing hydrometeors. Provided the core radial velocities are near zero the flare velocities depend on $w \sin\theta_r$ as predicted by Zrnić. When the core radial velocities are significantly nonzero the resulting flare velocities were usually, but not always, dominated by the $w \sin\theta_r$ term. Zrnić's equation predicts the flare velocities should approach the core radial velocities as the distance along the flare increases. Instead, it was observed that the flare velocities usually approach zero. As discussed in section 2, this may be more a result of how the pulse-pair Doppler processor computes the mean velocity for a broad flat Doppler spectrum than an error in the flare velocity equation.

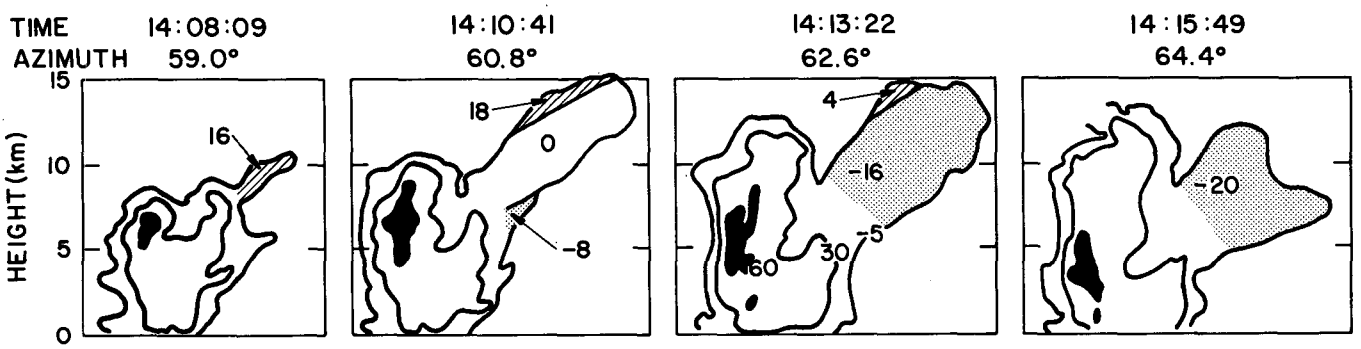

FIG. 7. The RHI displays of the evolution of a flare echo from CP-4 on 20 July 1986 near Huntsville, Alabama. Contours are reflectivity factor at −5, 30 and 60 dBZ_e. Positive Doppler velocities within the flare region are cross-hatched and negative velocities are stippled. Maximum approaching and receding velocities are indicated. The time and azimuth of each RHI are indicated. The azimuth was selected to correspond to the storm center.

The occurrence of a flare echo is radar wavelength dependent as it is observed more frequently at shorter wavelengths. As Zrnić proposed, this suggests non-Rayleigh scattering causes the flare. The Colorado data strongly suggest that scattering from large hail is the cause of the flare echo. Data from Alabama indicate that large raindrops may also produce flare echoes.

The likelihood that a flare echo is associated with large (≥2 cm) hail is sufficiently high in Colorado to justify issuing a severe storm warning. The use of this signature for large hail warnings outside Colorado is unclear. It is probably dependent on the freezing level height and the magnitude of the below-cloud base moisture. Researchers doing multiple Doppler analysis to generate wind fields in convective storms should be alert to this artifact since it would seriously contaminate synthesized wind fields. The unaware forecaster viewing a Doppler velocity display may be fooled into believing a large convergence of air is occurring into a storm. In addition, automated algorithms for detecting microbursts and convergent lines such as planned for the Next Generation Weather Radar Project and the Terminal Doppler Weather Radar Program are likely to generate false alarms if appropriate precautions are not taken to identify flare echoes.

Frequently the fall speed of the flare causing hydrometeors can be determined from the flare velocities. This can be used to great advantage for very short period forecasting of microbursts. For example, in the case of Fig. 7, the flare velocities changed from positive to strong negative, indicating the onset of a strong downdraft. A microburst was observed shortly after the flare velocities became strongly negative. The use of large approaching flare velocities, particularly when not caused by large falling hail, as a tool for forecasting microbursts warrants further study.

Acknowledgments. The authors are most grateful to Dr. Dusan Zrnić of the National Severe Storms Laboratory for advanced copies of his manuscript on the three-body scattering process, as well as numerous discussions on the subject, and review of an early version of this manuscript.

We thank Mr. Peter Neilley of the Massachusetts Institute of Technology, and Cindy Mueller, Cathy Kessinger, and Rita Roberts, all of NCAR, for their advice and review of the manuscript. We would also like to thank Drs. Bringi of Colorado State University, Gregory Forbes of Pennsylvania State University, Theodore Fujita of the University of Chicago, and Roger Wakimoto of the University of California at Los Angeles for permission to use the MIST radar data. The 1984 CP-4 data were made possible through the MAYPOLE program whose principal investigators were Drs. Bringi of Colorado State University and Thomas Seliga of Pennsylvania State University, and Dr. Paul Herzegh and Mr. Richard Carbone of NCAR. The 1983 CP-2 data were made available through NOAA/PROFS.

Our thanks to Maggie Miller who typed the manuscript and Carol Nicolaidis who provided editorial review.

APPENDIX

Flare Reflectivity Factor

Zrnić (1987) has derived the following equation for the reflectivity factor within the flare signature (Z_s):

$$Z_s = \frac{\pi^5 |K_i|^4 \theta_1^2 (R + r)^2 d^2 \sigma(\theta_r) F^2(\theta_r) Z_h^2}{r^3 \lambda^4 |K_w|^2 16 \ln 2}$$

where

$\|K_i\|$	the complex refractive index of the scatters
θ_1	the 3 dB antenna beam width
R	the distance from the radar to the scatters causing the flare
r	the distance from flare causing hydrometeors to the ground
d	the depth along the beam axis of the region containing the hydrometeors that cause the flare
$\sigma(\theta_r)$	the radar cross section per unit area of the ground at incident angle θ_r
$F^2(\theta_r)$	the function describing the angular dependence of the scattered power
Z_h	the effective reflectivity factor of scattering hydrometeors
λ	the radar wavelength
$\|K_w\|$	the complex refractive index of water.

In deriving this equation it is assumed that the ground scatters isotropically and the radar cross section of the ground is only weakly dependent on the incident angle of the scattering path to the ground. It is also assumed that $R + r$ is considerably greater than d.

The radar reflectivity factor in the flare is then dependent on $(R + r)^2/r^3$. The radar-received power (P_r) will then be dependent on r^{-3} since $\bar{P}_r$ is proportional to $1/[(R + r)^2]Z_s$ and the $(R + r)^2$ term will cancel.

REFERENCES

Aydin, K. A., T. A. Seliga and V. Balaji, 1986: Remote sensing of hail with a dual linear polarization radar. *J. Climate Appl. Meteor.*, **25**, 1475–1484.

Battan, L. J., 1973: *Radar Observations of the Atmosphere,* University of Chicago Press, 324 pp.

Bringi, V. N., T. A. Seliga and K. Aydin, 1984: Hail detection with a differential reflectivity radar. *Science,* **225,** 1145–1147.

Leitao, M. J., and P. A. Watson, 1984: Application of dual linearly polarized radar data to prediction of microwave path attenuation at 10–30 GHz. *Radio Sci.*, **19,** 209–221.

Lipschutz, R. C., J. F. Pratte and J. R. Smart, 1986: An operational Z_{DR}-based precipitation type/intensity product. In Preprint Vol. 3, *Joint Session 23rd Conf. on Radar Meteorology and Conf. on Cloud Physics,* Snowmass, Amer. Meteor. Soc., JP91–JP94.

Long, M. W., 1975: Radar Reflectivity of Land and Sea. Artech Houze, Inc., 385 pp.

Ulbrich, C. W., 1977: Doppler radar relationships for hail at vertical incidence. *J. Appl. Meteor.*, **16,** 1349–1359.

Wilson, J. W., and D. Reum, 1986: The "hail spike": reflectivity and velocity signature. In Preprint Vol. 1, *23rd Conference on Radar Meteorology,* Snowmass, Amer. Meteor. Soc., 62–65.

Zrnić, D. S., 1987: Three-body scattering produces precipitation signatures of special diagnostic value. *Radio Sci.*, **22,** 76–86.